

# Analysis of the dripping–jetting transition in compound capillary jets

M. A. HERRADA<sup>1</sup>, J. M. MONTANERO<sup>2</sup>,  
C. FERRERA<sup>1</sup> AND A. M. GAÑÁN-CALVO<sup>1†</sup>

<sup>1</sup>Departamento de Ingeniería Aeroespacial y Mecánica de Fluidos,  
Universidad de Sevilla, E-41092 Sevilla, Spain

<sup>2</sup>Departamento de Ingeniería Mecánica, Energética y de los Materiales,  
Universidad de Extremadura, E-06071 Badajoz, Spain

(Received 11 October 2009; revised 22 January 2010; accepted 23 January 2010)

We examine the behaviour of a compound capillary jet from the spatio-temporal linear stability analysis of the Navier–Stokes equations. We map the jetting–dripping transition in the parameter space by calculating the Weber numbers for which the convective/absolute instability transition occurs. If the remaining dimensionless parameters are set, there are two critical Weber numbers that verify Brigg’s pinch criterion. The region of absolute (convective) instability corresponds to Weber numbers smaller (larger) than the highest value of those two Weber numbers. The stability map is affected significantly by the presence of the outer interface, especially for compound jets with highly viscous cores, in which the outer interface may play an important role even though it is located very far from the core. Full numerical simulations of the Navier–Stokes equations confirm the predictions of the stability analysis.

---

## 1. Introduction

Compound capillary jets have a clear relevance for the production of microcapsules and hollow and coaxial microfibres. The production of microcapsules is of especial interest in a broad spectrum of applications and technological fields such as encapsulation of food additives, targeted drug delivery and special material processing. In these applications, the microcapsules contain an active agent surrounded by shell made up of materials such as polymers, carbohydrates, fats and waxes. Hollow and coaxial microfibres are of great interest for applications in material science.

Both microcapsules and microfibres are produced by stretching fluid interfaces down to the micrometre scale. One can distinguish two approaches for carrying out this process. In the first, the fluids are forced through orifices to get interfaces of sizes similar to those of the orifices (Umbanhowar, Prasad & Weitz 2000; Basaran 2002). This procedure yields monodisperse collections of capsules (Stone, Stroock & Adjari 2004), but is limited by the fact that the orifice may clog up for sizes below a few microns. The second approach is based on the use of either hydrodynamic (Gañán-Calvo 1998; Cohen *et al.* 2001; Bocanegra *et al.* 2005; Utada *et al.* 2005; Christopher & Anna 2007; He 2008) or electric (Loscertales *et al.* 2002; Barrero & Loscertales 2007; Gañán-Calvo & Montanero 2009) forces to stretch compound jets

† Email address for correspondence: amgc@us.es

down to a scale much smaller than the orifice size. The ultimate breakage of the jets can lead to the formation of micro- and nanocapsules with controlled structure and narrow size distributions (Gañán-Calvo 1998; Bocanegra *et al.* 2005). If the liquid solidifies before the jet breaks, hollow and coaxial nanofibres are obtained (Barrero & Loscertales 2007).

The upper part of figure 1 shows the axisymmetric flow-focusing configuration, which can be used to establish the compound capillary jet, which is the focus of this paper. A core (shell) fluid is injected through an inner (outer) capillary of representative diameter  $D_{1in}$  ( $D_{1out}$ ) at a flow rate  $Q_1$  ( $Q_2$ ). The representative diameters  $D_{1in}$  and  $D_{1out}$  are generally selected as the outer diameter of the inner tube and the inner diameter of the outer tube, respectively, since they define the gap through which the shell fluid flows. The resulting compound meniscus is stretched by a focusing air stream driven by a pressure drop  $\Delta P$  until a thin jet is emitted. Both the compound capillary jet and the gas current exit as a nearly parallel stream through an orifice of diameter  $D$  separated by a distance  $H$  from the capillaries. Figure 1 also shows typical compound capillary jets produced by an axisymmetric flow-focusing device in our laboratory. In the present work, we only examine the local axisymmetric stability of the compound jet, which is not significantly affected by the presence of the gas stream.

The quality and structure of the resulting capsules mainly depends on the compound jet breakup dynamics. Fundamentally, the compound jet behaviour is first determined by whether all the perturbations are convected downstream (convective instability) preserving a stable fluid ligament close to the orifice of the tapering meniscus (jetting regime), or some of them travel upstream while growing (absolute instability), which prevents the formation of the ligament (dripping regime) (Huerre & Monkewitz 1990). The relationship between the local convective and absolute instabilities and the jetting and dripping regimes has been reasonably well established: local convective instability is a prerequisite for getting stable jets of finite length in a co-flowing arrangement (Leib & Goldstein 1986; Gañán-Calvo, Herrada & Garstecki 2006; Gañán-Calvo *et al.* 2007; Guillot *et al.* 2007; Si *et al.* 2009).

Linear stability analysis can provide valuable predictions for the parameter values for which the convective/absolute (C/A) instability transition takes place. Chauhan *et al.* (2006) examined the appearance of absolute instability in inviscid compound jets. As the single-fluid jet, the compound jet becomes absolutely unstable below a critical Weber number, which increases as the outer surface tension increases. For convectively unstable states, the temporal analysis provides the wavelength of the perturbation responsible for the jet breakup. This analysis reveals the existence of the stretching and squeezing unstable modes (figure 2). These modes correspond to in-phase and out-of-phase deformations of the inner and outer interfaces, respectively (Sanz & Meseguer 1985; Chauhan *et al.* 2000). The film stretches in the stretching mode because the two interfaces grow in phase. On the contrary, the perturbations squeeze the fluid film in the squeezing mode because the two interfaces grow out of phase. The stretching and squeezing modes are mainly driven by capillary forces at the inner and outer interfaces, respectively. The growth rate of the stretching mode is real and positive for wavenumbers smaller than the inverse of core radius, and thus the mode is unstable for all waves with wavelength greater than the undisturbed core circumference. The squeezing mode has a real and positive growth rate for wavenumbers smaller than the inverse of the annulus radius, which implies that it is unstable for all disturbances with wavelength greater than the undisturbed outer circumference of the annulus. The stretching mode converges asymptotically to the

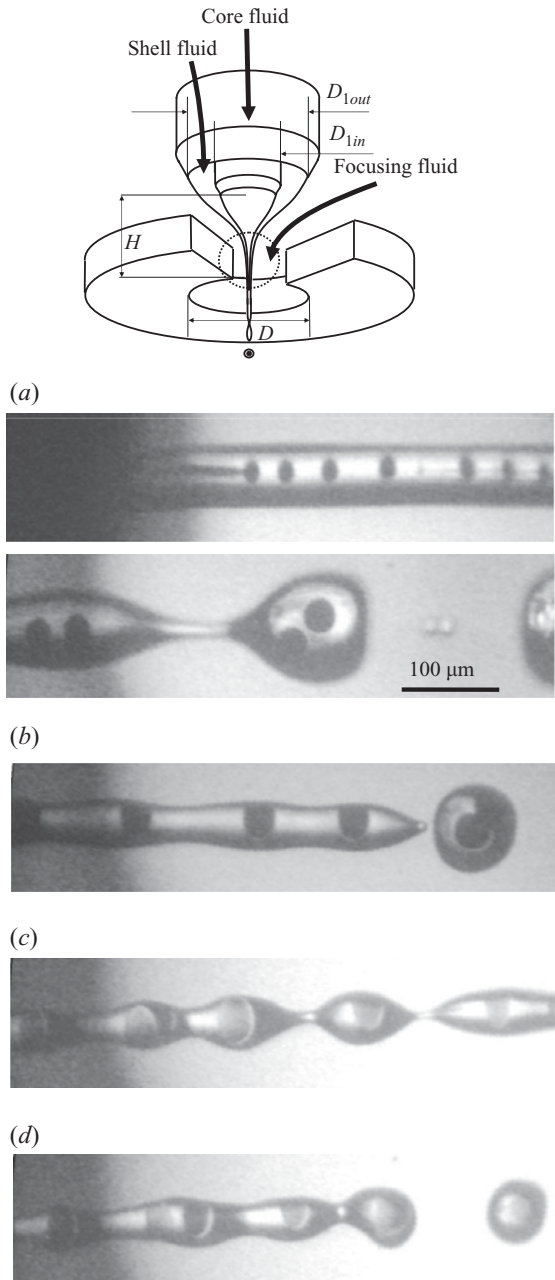


FIGURE 1. Axisymmetric flow-focusing device ( $D_{1in} = 400 \mu\text{m}$ ,  $D_{1out} = 700 \mu\text{m}$ ,  $D = 250 \mu\text{m}$ ,  $H = 220 \mu\text{m}$ ) used in the illustrative experiments shown below. The focusing, shell and core fluids were compressed air, silicone oil of  $0.005 \text{ Pa s}$  in viscosity and a mixture of 80% water + 20% black ink with traces ( $\sim 0.1\%$ ) of Tween 80, respectively. The values of the control parameters were the following: (a)  $\Delta P = 3 \text{ kPa}$ ,  $Q_1 = 0.5 \text{ mL h}^{-1}$ ,  $Q_2 = 30 \text{ mL h}^{-1}$  (multi-vesicle capsules); (b)  $\Delta P = 3 \text{ kPa}$ ,  $Q_1 = 1 \text{ mL h}^{-1}$ ,  $Q_2 = 30 \text{ mL h}^{-1}$  (mixed capsules of one and two cores); (c)  $\Delta P = 3 \text{ kPa}$ ,  $Q_1 = 4 \text{ mL h}^{-1}$ ,  $Q_2 = 30 \text{ mL h}^{-1}$  (single core capsules: the outer jet breakup is modulated by the core content); and (d)  $\Delta P = 5 \text{ kPa}$ ,  $Q_1 = 4 \text{ mL h}^{-1}$ ,  $Q_2 = 30 \text{ mL h}^{-1}$  (higher pressure drop inducing some irregularities).

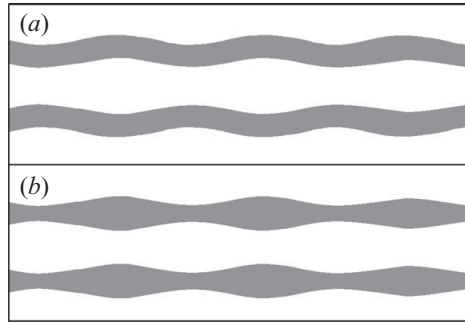


FIGURE 2. Sketch of the (a) stretching and (b) squeezing modes.

only unstable mode of a single jet (Tomotika 1935) as the outer interface departs from the inner one, and it dominates the breakup process because its maximum growth rate is larger than that of the squeezing mode (Sanz & Meseguer 1985; Chauhan *et al.* 2000).

Nonlinear effects may modify not only quantitatively but also qualitatively both the jetting–dripping transition and the breakup process in the jetting regime (Suryo, Doshi & Basaran 2006). For instance, numerical solutions of a one-dimensional model show that the jet breakup may be caused by a squeezing motion of the interfaces for highly viscous cores (Craster, Matar & Papageorgiou 2005). In the highly viscous annulus case, the simulations demonstrate the possibility of breakup of either the core or the annulus, depending on the initial ratio of the radii (Craster *et al.* 2005). Experiments (see e.g. figure 1) confirm the intricate dependence of the capsule structure on the governing parameters, showing the fundamental role of the initial ratio of the radii, the most unstable perturbation wavelength and its spatio-temporal growth rate (Bocanegra *et al.* 2005). A certain desired capsule structure predicted from the simple conservation of mass principle applied to the compound jet would be compromised or destroyed if any of the jet components breaks up unexpectedly. In this sense, convective instability may be the adequate regime to massively produce microcapsules from compound jets in a controlled way. It is, therefore, of fundamental importance to determine the operating conditions that prevent absolute instability and thus guarantee convective instability.

In this paper, we carry out a linear spatio-temporal stability analysis of a viscous compound capillary jet to map out the parameter regions of convective and absolute instabilities. This analysis is validated for some configurations by direct volume-of-fluid numerical simulations. The method is briefly described in §2. The results of the linear stability analysis and full numerical simulations are presented in §3. The conclusions are given in §4.

## 2. Method

### 2.1. Linear stability analysis

Consider a compound capillary jet consisting of a cylindrical core of radius  $R_1$ , density  $\rho_1$  and viscosity  $\mu_1$ , flowing inside an annulus of outer radius  $R_2$ , density  $\rho_2$  and viscosity  $\mu_2$ . We assume that axial momentum is diffused throughout the entire jet, and thus the two fluids move with the same velocity  $V$ . This occurs for moderately and highly viscous fluids immediately behind the emitting section and for low-viscosity fluids in a region sufficiently far from the emitting section. The

surface tensions of the inner and outer interfaces are  $\gamma_1$  and  $\gamma_2$ , respectively. The compound jet is moving inside a gas of negligible density and viscosity. Below, we make all the variables dimensionless using  $R_1$ ,  $V$ ,  $R_1/V$  and  $\rho_1 V^2$  as the characteristic length, velocity, time and pressure, respectively. The jet behaviour can be described in terms of the ratios of radii  $R \equiv R_2/R_1$ , densities  $\rho \equiv \rho_2/\rho_1$ , viscosities  $\mu \equiv \mu_2/\mu_1$  and surface tensions  $\gamma \equiv \gamma_2/\gamma_1$ , and in terms of the Reynolds  $Re \equiv \rho_1 V R_1/\mu_1$  and Weber  $We = \rho_1 V^2 R_1/\gamma_1$  numbers.

Using a Lagrangian frame of reference solidly moving with both fluids, we propose the following dependence for the velocity  $\mathbf{v}_j(\mathbf{r}, t)$  and pressure  $p_j(\mathbf{r}, t)$  fields, and for the positions  $f_j(\theta, z, t)$  of the interfaces:

$$\mathbf{v}_j(\mathbf{r}, t) = \varepsilon \{U_j(r), V_j(r), W_j(r)\} e^{i(m\theta + kz - \omega t)} + \text{c.c.}, \quad (2.1a)$$

$$p_j(\mathbf{r}, t) - \frac{\delta_{j1}}{We} = \varepsilon P_j(r) e^{i(m\theta + kz - \omega t)} + \text{c.c.}, \quad (2.1b)$$

$$f_j(\theta, z, t) - R^{\delta_{j2}} = \varepsilon F_j e^{i(m\theta + kz - \omega t)} + \text{c.c.} \quad (2.1c)$$

In (2.1a) and (2.1b),  $j=1$  and  $2$  denote the core and annulus fluid domains, respectively, while in (2.1c) they denote the inner and outer interfaces, respectively. In addition,  $m$  is the azimuthal wavenumber,  $k = k_r + ik_i$  is the axial wavenumber,  $\omega = \omega_r + i\omega_i$  is the frequency,  $\delta_{ij}$  is the Kronecker delta and c.c. denotes complex conjugate.

Introducing these perturbations into the incompressible Navier–Stokes equations and neglecting terms in  $\varepsilon^2$ , we get

$$U'_j + U_j/r + imV_j/r + ikW_j = 0, \quad (2.2a)$$

$$-\rho^{\delta_{j2}} i\omega U_j + P'_j = \frac{\mu^{\delta_{j2}}}{Re} \left[ U''_j + U'_j/r - (m^2 + 1)U_j/r^2 - k^2 U_j - 2imV_j/r^2 \right], \quad (2.2b)$$

$$-\rho^{\delta_{j2}} i\omega V_j + imP_j/r = \frac{\mu^{\delta_{j2}}}{Re} \left[ V''_j + V'_j/r - (m^2 + 1)V_j/r^2 - k^2 V_j + 2imU_j/r^2 \right], \quad (2.2c)$$

$$-\rho^{\delta_{j2}} i\omega W_j + ikP_j = \frac{\mu^{\delta_{j2}}}{Re} \left( W''_j + W'_j/r - m^2 W_j/r^2 - k^2 W_j \right), \quad (2.2d)$$

where the primes denote derivative with respect to  $r$ . The general solution to (2.2), verifying the regularity conditions

$$U_1(0) = V_1(0) = W'_1(0) = 0 \text{ for } m = 0, \quad U_1(0) + iV_1(0) = W_1(0) = 0 \text{ for } m = 1, \quad (2.3a)$$

$$U_1(0) = V_1(0) = W_1(0) = 0 \text{ for } m \geq 2, \quad (2.3b)$$

is

$$U_j(r) = ic_{j1} I'_m(kr) + ic_{j2} I'_m(k_j r) + im c_{j3} \frac{I_m(k_j r)}{k_j r} + \delta_{j2} \left[ id_1 K'_m(kr) + id_2 K'_m(k_2 r) + im d_3 \frac{K_m(k_2 r)}{k_2 r} \right], \quad (2.4a)$$

$$V_j(r) = -m c_{j1} \frac{I_m(kr)}{kr} - m c_{j2} \frac{I_m(k_j r)}{k_j r} - c_{j3} I'_m(k_j r) + \delta_{j2} \left[ -m d_1 \frac{K_m(kr)}{kr} - m d_2 \frac{K_m(k_2 r)}{k_2 r} - d_3 K'_m(k_2 r) \right], \quad (2.4b)$$

$$W_j(r) = -c_{j1} I_m(kr) - c_{j2} k_j \frac{I_m(k_j r)}{k} + \delta_{j2} \left[ -d_1 K_m(kr) - d_2 k_j \frac{K_m(k_j r)}{k} \right], \tag{2.4c}$$

$$P_j(r) = -\frac{\rho^{\delta_{j2}} \omega c_{j1}}{k} I_m(kr) + \delta_{j2} \left[ -\frac{\rho \omega d_1}{k} K_m(kr) \right]. \tag{2.4d}$$

Here,  $j=1$  and  $2$  denote the core and annulus fluid domains, respectively, and  $I_m$  and  $K_m$  are the modified Bessel functions of the first and second kind, respectively. In addition,  $k_1 = \pm [k^2 - i\omega Re]^{1/2}$ ,  $k_2 = [k^2 - i\omega Re \rho/\mu]^{1/2}$ , and  $\{c_{j1}, c_{j2}, c_{j3}, d_1, d_2, d_3\}$  are nine arbitrary constants. It must be noted that (2.4) is symmetric with respect to  $k_1$  (i.e. is invariant under the change  $k_1 \rightarrow -k_1$ ).

The non-slip condition  $\{U_1 = U_2, V_1 = V_2, W_1 = W_2\}$  at the inner interface  $r = 1$  yields a linear system of equations that allows one to obtain  $\{d_1, d_2, d_3\}$  in terms of  $\{c_{j1}, c_{j2}, c_{j3}\}$ . The condition of dynamical equilibrium at the inner interface  $r = 1$  for the normal and two tangential components leads to

$$P_1 - P_2 + \frac{i(1 - m^2 - k^2)}{We \omega} U_1 = \frac{2}{Re} (U'_1 - \mu U'_2), \tag{2.5a}$$

$$W'_1 + ikU_1 = \mu(W'_2 + ikU_2), \tag{2.5b}$$

$$imU_1 + V'_1 - V_1 = \mu(imU_2 + V'_2 - V_2), \tag{2.5c}$$

where we use the kinematic compatibility condition  $F_1 = iU_j(1)/\omega$  to eliminate  $F_1$  from (2.5a). Analogously, the condition of dynamical equilibrium at the outer interface  $r = R$  for the normal and two tangential components leads to

$$P_2 + \frac{i[(1 - m^2)/R^2 - k^2]}{(We/\gamma) \omega} U_2 = \frac{2\mu}{Re} U'_2, \tag{2.6a}$$

$$W'_2 + ikU_2 = 0, \tag{2.6b}$$

$$imU_2 + V'_2 - V_2 = 0. \tag{2.6c}$$

The sets of (2.5) and (2.6) constitute a linear system of equations for  $\{c_{j1}, c_{j2}, c_{j3}\}$ . The solvability condition  $\text{Det}(\Delta_{ij}) = 0$ , with  $\Delta_{ij}$  being the  $6 \times 6$  matrix associated with that the system of equations, yields the dispersion relation in the Lagrangian frame of reference. To determine the values of the parameters for which the basic flow undergoes a C/A instability transition, we should explore the response of the system to perturbations characterized by a complex axial wavenumber  $k$  (spatio-temporal analysis), observed by a fixed observer (Huerre & Monkewitz 1990). To change the frame of reference from a travelling observer to a fixed one, the wave frequency  $\omega$  should be replaced by  $\omega - k$  in the calculations (Leib & Goldstein 1986). The result is

$$D_m(k, \omega; R, \rho, \mu, \gamma, Re, We) = 0. \tag{2.7}$$

An explicit expression of (2.7) cannot be provided. A MATHEMATICA notebook containing the dispersion relation can be obtained upon request from the authors.

Non-axisymmetric perturbations ( $m \neq 0$ ) have an aerodynamic origin. If a (single or compound) jet co-flows with an outer stream with non-negligible density moving with a different velocity, then a perturbation at the interface causes the outer stream

to accelerate as it passes a crest, lowering the dynamic pressure at that point. This encourages the crest to increase in size. This instability mechanism is absent in the fluid configuration considered in the present work because the outer stream is assumed to have a negligible density. For this reason, we shall focus on axisymmetric  $m = 0$  perturbations.

The critical Weber numbers  $We^*$  corresponding to the C/A instability transitions are determined by a spatio-temporal analysis of the dispersion relation (2.7). We calculate these critical Weber numbers  $We^*$  as those values of  $We$  for which Brigg's pinch condition (Briggs 1964; Huerre & Monkewitz 1990) is satisfied. This condition establishes that there must be at least one pinching of a  $k^+$  and a  $k^-$  spatial branch with  $\omega_i = 0$ , where  $k^+$  is the path of  $D_m = 0$  in the complex  $k$ -plane that moves into the  $k_i > 0$  half-plane as  $\omega_i$  increases, while the  $k^-$  branch always remains in the  $k_i < 0$  half-plane as  $\omega_i$  increases. If  $k^+$  crosses the  $k_r$  axis through the point  $k_r = 1$  ( $k_r = 1/R$ ), the C/A instability transition is associated with the stretching (squeezing) mode.

The wave frequencies were calculated as the roots of the transcendental equation (2.7) for fixed values of the wavenumber and the rest of parameters characterizing the problem. These roots were found numerically by means of the Newton–Raphson method. Mapping the convective and absolute instability regions over the whole parameter space  $\{R, \rho, \mu, \gamma, Re, We\}$  requires a very long computing time owing to the high dimensionality and the complexity of (2.7). To facilitate the calculations, we used a Chebyshev spectral collocation technique based on the approach developed by Khorrami (1991) for the stability analysis of swirling flows in pipes. This method has been successfully used to analyse, for instance, the stability of low-density and low-viscosity fluid jets and spouts in an unbounded co-flowing liquid environment (Gañán-Calvo *et al.* 2006). Preliminary explorations of the dispersion relation over the  $k$ -plane were carried out by the spectral technique to find approximately the saddle points verifying Brigg's criterion. The results were used as initial guesses to determine the critical Weber numbers from the exact dispersion relation (2.7).

## 2.2. Numerical simulations

In order to validate our stability analysis, we carried out six ‘numerical experiments’ by means of the volume-of-fluid method implemented by the commercial solver FLUENT v 6.3. Details of the method can be found elsewhere (Herrada *et al.* 2008). We simulated the flow of a compound capillary jet surrounded by a fluid with viscosity and density 100 times smaller than the corresponding values of the annulus. The compound jet and the surrounding gas were enclosed by a cylindrical tube of radius  $R_{ext} = 8$  and length  $L = 100$ . Appropriate boundary conditions were imposed to get results under conditions similar to those of the stability analysis. Specifically, a uniform axial velocity profile at the tube inlet ( $z = 0$ ) was imposed for the three phases, while symmetric and slip conditions were used at the jet axis ( $r = 0$ ) and the tube wall ( $r = R_{ext}$ ), respectively. Finally, outflow conditions are considered at the tube outlet ( $z = L$ ). The results were computed with a time step  $\Delta t = 0.2$  in a uniform mesh with  $N = 80 \times 1000$  points. We verified that similar results are obtained for larger values of  $R_{ext}$ ,  $L$ ,  $\Delta t^{-1}$  and  $N$ .

In the simulations, we first set the values of the parameters characterizing the fluid configuration. Then, the simulation starts by injecting the two liquids and the surrounding gas of negligible density and viscosity in the empty tube. The system evolves until reaching a quasi-periodic regime. If a compound jet long compared to its diameter is formed in that regime, then the regime corresponds to steady jetting.

On the contrary, if drops are ejected immediately behind the tube inlet (figure 6), it corresponds to dripping (figure 7).

### 3. Results

#### 3.1. Linear stability analysis

Because of the high dimensionality of the parameter space, we shall only consider capillary jets consisting of fluids with equal kinematic viscosities ( $\rho = \mu$ ). In general, there are at least two saddle points for a given set of the flow parameters. The dominant saddle point is the one with the largest absolute growth rate. Here, we call ‘critical’ Weber numbers those values for which a saddle point verifies Brigg’s pinch criterion. If that saddle point is the dominant one, then the critical Weber number is also the ‘transitional’ Weber number. The transitional Weber number indicates when the true (physical) C/A instability transition takes place.

In order to clarify the difference between the critical and transitional Weber numbers, we consider here a virtual experiment. Assume that all the parameters characterizing the fluid configuration are fixed in the experiment excepting the  $We$ , which can be varied at will. For sufficiently large values of  $We$ , steady jetting is encountered. Decreasing progressively  $We$  results in a ‘transitional’ Weber number for which the transition from the jetting to the dripping regimes occurs. This transitional Weber number is the value for which the ‘dominant’ saddle point (i.e. that with the largest absolute growth rate) of the dispersion relation verifies Brigg’s pinch criterion. One can keep on decreasing the Weber number in the dripping regime. In this case, other saddle points (different from the dominant one) may also verify Brigg’s pinch criterion. The ‘critical’ Weber numbers for which this occurs do not correspond to any true (physical) C/A instability transition.

Figure 3 shows the critical Weber number as a function of  $R$  for a liquid–liquid configuration ( $\rho = 1$ ) and different choices of  $Re$  and  $\gamma$ . The comparison with the results obtained from the Chebyshev spectral collocation technique (circles) for some cases shows the accuracy of that technique. If the remaining parameters are set, there are two critical Weber numbers (solid and dashed lines). In both cases, the C/A instability transition is associated with the stretching mode. The transitional Weber number is the higher value of those two critical Weber numbers. For that Weber number, the growth rate of the dominant saddle point becomes positive. The region of absolute (convective) instability corresponds to Weber numbers smaller (larger) than the transitional Weber number.

As can be observed in figure 3, one of the critical Weber numbers (dashed lines) determines the true C/A instability transition for large  $R$ . It tends to the transitional Weber number for a jet co-flowing with an unbounded stream (Gañán-Calvo *et al.* 2006, 2007) as  $R \rightarrow \infty$ . There is a radius ratio  $R^*$  below which the other critical Weber number (solid lines) becomes dominant. This Weber number increases as  $R$  decreases but it does not diverge as  $R \rightarrow 1$ . In this limit, the two interfaces overlap, and the compound jet behaves as a single jet in vacuum with an effective surface tension  $\gamma_1 + \gamma_2$ . In fact, we verified that the transitional value of  $We/(1 + \gamma)$  obtained for  $R \rightarrow 1$  coincides with that calculated by Leib & Goldstein (1986) for a single jet in vacuum. The results obtained for  $R \rightarrow 1$  show that compound jets with an infinitely thin annulus could, in principle, be produced with a co-flowing configuration. This behaviour resembles the ‘unconditional jetting’ phenomenon described by Gañán-Calvo *et al.* (2007) and Gañán-Calvo (2008), where infinitely thin jets are convectively unstable over a critical finite capillary number,  $Ca = We/Re$ . This means that, in



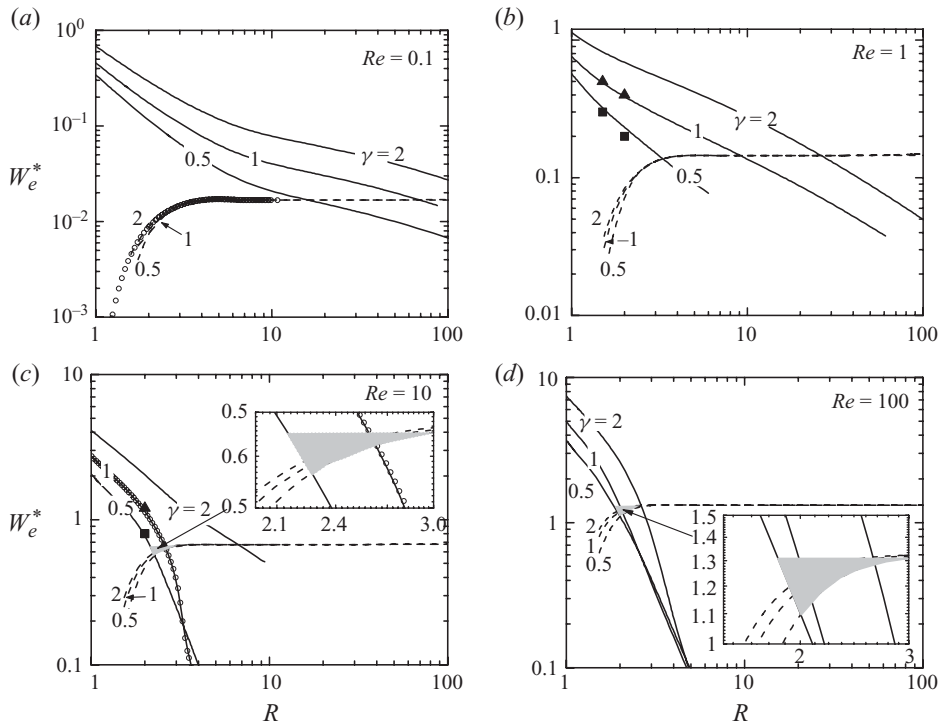


FIGURE 3. Critical Weber number  $We^*$  as a function of the radius ratio  $R$  for  $\rho = \mu = 1$ ,  $Re = 0.1, 1, 10$  and  $100$ , and  $\gamma = 0.5, 1$  and  $2$ . The solid and dashed lines correspond to the two critical Weber numbers. The transitional Weber number, which indicates the true C/A instability transition, is the larger value of those two critical Weber numbers. The circles are solutions obtained from the Chebyshev spectral collocation technique for  $Re = 0.1$  and  $\gamma = 2$ , and  $Re = 10$  and  $\gamma = 1$ . The shaded areas in the graphs for  $Re = 10$  and  $100$  are the intervals of  $R$  for which the presence of an outer interface with  $\gamma = 0.5$  favours the jetting regime. The triangles (squares) correspond to the simulations in the jetting (dripping) regime for  $\gamma = 1$ .

principle, very thin jets could be produced if the source used to emit them were stable under such condition (Gañán-Calvo & Montanero 2009).

Essentially, the outer interface reduces the parameter region in which the compound jet is convectively unstable. As in the inviscid case (Chauhan *et al.* 2006), the transitional Weber number increases with  $\gamma$ . In other words, the outer interface favours the transition from the jetting to the dripping regimes. There are some narrow parameter windows (see e.g. the shaded areas in the graphs for  $Re = 10$  and  $100$ ) that constitute exceptions to the above rule. In figure 3, the intersection between the solid and dashed lines at  $R = R^*$  moves towards larger values of  $R$  as  $\gamma$  increases or  $Re$  decreases. This means that the influence of the outer interface on the stability map increases as it becomes stiffer or the core becomes more viscous. Indeed, for  $Re = 0.1$  and  $\gamma = 2$ , the transitional Weber number always exceeds the value corresponding to the unbounded outer stream. This implies that, under certain conditions, the outer interface might affect the stability of the inner jet even though they were very far from each other. In that case, the dispersion relations calculated for jets moving in unbounded liquids (see e.g. Tomotika 1935; Funada, Joseph & Yamashita 2004; Gañán-Calvo *et al.* 2006, 2007; Montanero & Gañán-Calvo 2008; Utada *et al.* 2008) may lead to inaccurate predictions for the jetting–dripping transition. It must be

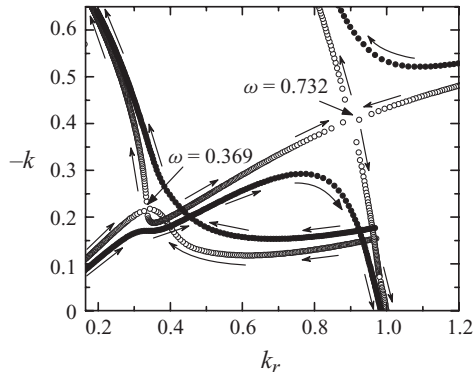


FIGURE 4. Double pinching with zero growth rate for  $\rho = \mu = \gamma = 1$ ,  $Re = 10$ ,  $R = 2.622$  and  $We = 0.6338$ . The open and filled symbols correspond to spatial branches with  $\omega_i = 0$  and  $0.02$ , respectively. The arrows indicate the direction in which  $\omega_r$  increases.

noted that this lack of accuracy does not occur in the (simpler) temporal analysis of the dispersion relation, in which one can neglect the effect of distant boundaries and still obtain accurate results for the temporal growth rates. For instance, the stretching mode solution for  $R_2/R_1 \gtrsim 10$  matches that of Tomotika (1935) (see e.g. figure 7 in Chauhan *et al.* 2000).

Interestingly, the fact that the presence of a distant outer boundary can affect the absolute instability of the system has been observed in other configurations, such as single jets and wakes (Juniper 2007; Healey 2008), and boundary and mixing layers (Healey 2007, 2009). In all these cases, the fluids were inviscid and confined by rigid boundaries. Our results show that the same effect can be observed for viscous fluids limited by an outer interface, which indicates that this unexpected behaviour could be widespread.

For a given set of parameters, there are at least two saddle points of (2.7) in the  $k$  complex plane associated with the stretching mode. For  $R > R^*$ , one of them has a growth rate greater than the other, while the opposite occurs for  $R < R^*$ . The two saddle points have zero growth rate for  $R = R^*$  and  $We = We^*$ , and thus verify Brigg's pinch criterion (Briggs 1964) simultaneously. This peculiar situation is illustrated in figure 4, where one can observe how the saddle points 'couple each other' through one of the spatial branches. This phenomenon has not previously been observed in capillary systems. It has a mathematical character, because it corresponds to a jetting–dripping transition that could not be distinguished from others experimentally.

The case  $\rho, \mu \gg 1$  is relevant for applications such as the production of hollow microfibres from co-flowing systems. Figure 5 illustrates the results for  $\rho = \mu = 10^3$ ,  $\gamma = 1$ , and different values of the Reynolds number. The results for  $Re = 100$  are qualitatively the same as those for liquid–liquid jets: there are two critical Weber numbers: one determines the jetting–dripping transition for large  $R$ , while the other is dominant for small  $R$ . Interestingly, only one critical Weber number was found for  $Re = 0.1, 1$  and  $10$  within the interval of  $R$  explored. In all the cases, the transitional Weber number does not diverge for  $R \rightarrow 1$ , so that infinitely thin hollow fibres could in principle be produced by a co-flowing arrangement.

### 3.2. Numerical simulations

We performed numerical simulations to illustrate the breakup process of the compound jet for some selected cases. It must be noted that simulations for large

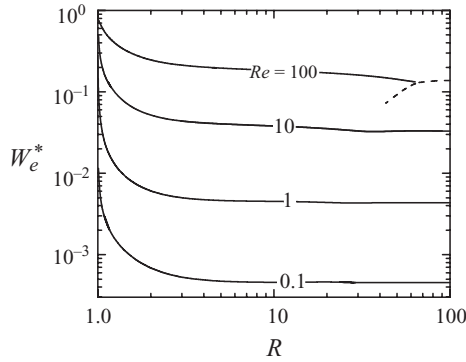


FIGURE 5. Critical Weber number  $We^*$  as a function of the radius ratio  $R$  for  $\rho = \mu = 10^3$ ,  $Re = 0.1, 1, 10$  and  $100$ , and  $\gamma = 1$ . The solid and dashed lines correspond to the two critical Weber numbers found for each case. The transitional Weber number, which indicates the true C/A instability transition, is the larger value of those two critical Weber numbers.

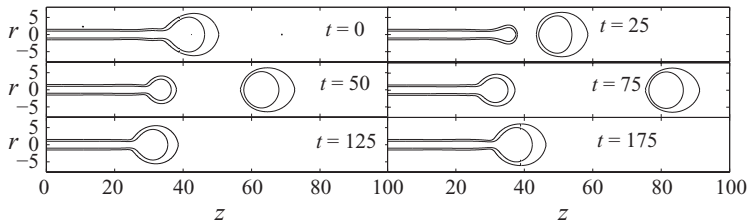


FIGURE 6. Drop formation in the jetting regime for  $\rho = \mu = Re = \gamma = 1$ ,  $R = 1.5$  and  $We = 0.5$ . The figure shows snapshots over an interval of time that approximately corresponds to the drop formation period.

$Re$  require refined meshes and longer tubes because of the slower growth of the perturbations in the jetting regime. In addition, the agreement between the linear stability analysis and the simulations is expected to improve as  $Re$  decreases because the relative magnitude of the nonlinear convective term decreases with  $Re$ . Finally, the computing time increases sharply with  $R$ . For these reasons, we considered the intermediate cases  $Re = 1$  and  $10$ ,  $\gamma = 1$  and  $R = 1.5$  and  $2$ .

Figure 6 allows one to visualize the drop formation cycle in the jetting regime. The instants of time  $t = 0$  and  $175$  approximately correspond to the same state in the cycle, just before the emission of the compound drop. One can observe how the drop forms between those instants of time due to the growth of a stretching perturbation, consistent with the prediction of the linear temporal stability analysis (Chauhan *et al.* 2000). Because its amplitude is small compared with the size of the incipient drop, it cannot be appreciated in the figure. The stretching perturbation cannot travel upstream and thus a ligament remains practically stable for  $z \lesssim 30$ . Figure 7 shows the drop formation in the dripping regime. In this case, the perturbations propagate upstream and the compound jet drips periodically at the tube inlet. The drops are the consequence of a stretching process too, as predicted by our spatio-temporal stability analysis. The triangles and squares in figure 3 correspond to six simulations in the jetting and dripping regimes, respectively. As can be observed, they are consistent with the predictions for the C/A instability transition.

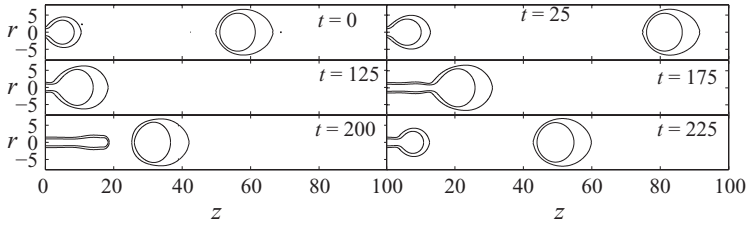


FIGURE 7. Drop formation in the dripping regime for  $\rho = \mu = Re = \gamma = 1$ ,  $R = 1.5$  and  $We = 0.3$ . The figure shows snapshots over an interval of time that approximately corresponds to the drop formation period.

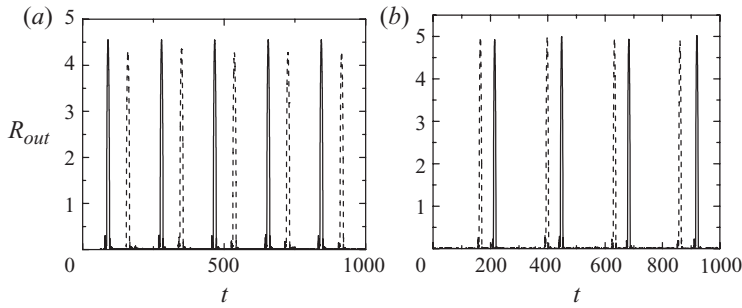


FIGURE 8. Radius  $R_{out}$  of the inner drop at the tube outlet as a function of time in the periodic regime for  $\Omega = 0.3$  (solid lines) and  $0.5$  (dashed lines). The flow parameters in (a) and (b) are those of figures 5 and 6, respectively.

The response of the compound jet to external perturbations is qualitatively different in the jetting and dripping regimes. In the jetting regime, the jet evolution can be significantly altered by introducing unstable modes with small but finite initial amplitudes, which may ultimately dominate the breakup process. On the contrary, the jet dynamics in the dripping regime are essentially determined by the absolute instability, and the effects of small external perturbations are generally negligible. Figures 8(a) and 8(b) show the simulation results for the flow perturbed artificially by introducing a uniform harmonic perturbation of frequency  $\Omega$  in the velocity distribution at the tube inlet. The amplitude of the perturbation was 1% of the velocity magnitude. The figures show the radius  $R_{out}$  of the inner drop at the tube outlet in the periodic regime, defined as

$$R_{out}(t) = \sqrt{2 \int_0^8 \alpha_1(t, r) r \, dr}, \tag{3.1}$$

where  $\alpha_1(t, r)$  is the volume fraction of the inner liquid at the tube outlet. Figures 8(a) and 8(b) show the results obtained for  $\Omega = 0.3$  (solid lines) and  $0.5$  (dashed lines). The flow parameters in figures 8(a) and 8(b) are those of figures 6 and 7, respectively, corresponding to the jetting and dripping regimes. In the jetting regime, the breakup process depends significantly on the external perturbation frequency: smaller inner drops were produced with a higher frequency for  $\Omega = 0.5$ . However, the jet dynamics are almost independent of  $\Omega$  in the dripping regime, which shows that the breakup process is dominated by the intrinsic dynamics of the system in this case.

#### 4. Conclusions

The jetting–dripping transition in compound capillary jets has been analysed from the linear stability analysis. The existence of an outer interface generally favours the absolute instability of the stretching mode leading to the dripping regime. The results for liquid–liquid jets (figure 3) show that this effect increases with the outer interface surface tension and/or the jet core viscosity. For moderately low Reynolds numbers ( $Re \lesssim 0.1$ ), the role played by the outer interface is noticeable even though it is located very far from the core ( $R \gtrsim 100$ ), in contrast to what was naturally assumed in previous works (see e.g. Tomotika 1935; Funada *et al.* 2004; Gañán-Calvo *et al.* 2006, 2007; Montanero & Gañán-Calvo 2008; Utada *et al.* 2008). The transitional Weber number remains bounded in the limit  $R \rightarrow 1$ , which implies that the jetting regime can be found in compound jets with an infinitely thin annulus. The same result was found for the gas–liquid configuration (figure 5). This is analogous to the ‘unconditional jetting’ phenomenon (Gañán-Calvo *et al.* 2007; Gañán-Calvo 2008), where infinitely thin jets can be produced above a finite critical capillary number. The numerical simulations of the nonlinear Navier–Stokes equations carried out in this work are in agreement with the above conclusions.

Partial support from the Ministry of Science and Education (Spain) through grant DPI2007-63559 is gratefully acknowledged.

#### REFERENCES

- BARRERO, A. & LOSCERTALES, I. G. 2007 Micro- and nanoparticles via capillary flows. *Annu. Rev. Fluid Mech.* **39**, 89–106.
- BASARAN, O. A. 2002 Small-scale free surface flows with breakup: drop formation and emerging applications. *AIChE J.* **48**, 1842–1848.
- BOCANEGRA, R., SAMPEDRO, J. L., GAÑÁN-CALVO, A. M. & MARQUEZ, M. 2005 Monodisperse structured multi-vesicle microencapsulation using flow-focusing and controlled disturbance. *J. Microencapsul.* **22**, 745–759.
- BRIGGS, R. J. 1964 *Electron-Stream Interaction with Plasmas*. MIT Press.
- CHAUHAN, A., MALDARELLI, C., PAPAGEORGIOU, D. T. & RUMSCHITZKI, D. S. 2000 Temporal instability of compound threads and jets. *J. Fluid Mech.* **420**, 1–25.
- CHAUHAN, A., MALDARELLI, C., PAPAGEORGIOU, D. T. & RUMSCHITZKI, D. S. 2006 The absolute instability of an inviscid compound jet. *J. Fluid Mech.* **549**, 81–98.
- CHRISTOPHER, G. F. & ANNA, S. L. 2007 Microfluidic methods for generating continuous droplet streams. *J. Phys. D: Appl. Phys.* **40**, R319–R336.
- COHEN, I., LI, H., HOUGLAND, J. L., MRKSICH, M. & NAGEL, S. R. 2001 Using selective withdrawal to coat microparticles. *Science* **292**, 265–267.
- CRASTER, R. V., MATAR, O. K. & PAPAGEORGIOU, D. T. 2005 On compound liquid threads with large viscosity contrasts. *J. Fluid Mech.* **533**, 95–124.
- FUNADA, T., JOSEPH, D. D. & YAMASHITA, S. 2004 Stability of a liquid jet into incompressible gases and liquids. *Intl J. Multiphase Flow* **30**, 1279–1310.
- GAÑÁN-CALVO, A. M. 1998 Generation of steady liquid microthreads and micron-sized monodisperse sprays in gas streams. *Phys. Rev. Lett.* **80**, 285–288.
- GAÑÁN-CALVO, A. M. 2008 Unconditional jetting. *Phys. Rev. E* **78**, 026304.
- GAÑÁN-CALVO, A. M., GONZÁLEZ-PRIETO, R., RIESCO-CHUECA, P., HERRADA, M. A. & FLORES-MOSQUERA, M. 2007 Focusing capillary jets close to the continuum limit. *Nature Phys.* **3**, 737–742.
- GAÑÁN-CALVO, A. M., HERRADA, M. A. & GARSTECKI, P. 2006 Bubbling in unbounded coflowing liquids. *Phys. Rev. Lett.* **96**, 124504 (1–4).
- GAÑÁN-CALVO, A. M. & MONTANERO, J. M. 2009 Revision of capillary cone-jet physics: electrospray and flow focusing. *Phys. Rev. E* **79**, 066305 (1–18).

- GUILLOT, P., COLIN, A., UTADA, A. S. & AJDARI, A. 2007 Stability of a jet in confined pressure-driven biphasic flows at low Reynolds numbers. *Phys. Rev. Lett.* **99**, 104502.
- HE, Y. 2008 Application of flow-focusing to the breakup of an emulsion jet for the production of matrix-structured microparticles. *Chem. Engng Sci.* **63**, 2500–2507.
- HEALEY, J. J. 2007 Enhancing the absolute instability of a boundary layer by adding a far-way plate. *J. Fluid Mech.* **579**, 29–61.
- HEALEY, J. J. 2008 Inviscid axisymmetric absolute instability of swirling jets. *J. Fluid Mech.* **613**, 1–33.
- HEALEY, J. J. 2009 Destabilizing effects of confinement on homogeneous mixing layers. *J. Fluid Mech.* **623**, 241–271.
- HERRADA, M. A., GAÑÁN-CALVO, A. M., OJEDA-MONGE, A., BLUTH, B. & RIESCO-CHUECA, P. 2008 Liquid flow focused by a gas: jetting, dripping, and recirculation. *Phys. Rev. E* **78**, 036323 (1–16).
- HUERRE, P. & MONKEWITZ, P. A. 1990 Local and global instabilities in spatially developing flows. *Annu. Rev. Fluid Mech.* **22**, 473–537.
- JUNIPER, M. P. 2007 The full response of two-dimensional jet/wake flows and implications for confinement. *J. Fluid Mech.* **590**, 163–185.
- KHORRAMI, M. R. 1991 A Chebyshev spectral collocation method using a staggered grid for the stability of cylindrical flows. *Intl J. Numer. Methods Fluids* **12**, 825–833.
- LEIB, S. J. & GOLDSTEIN, M. E. 1986 The generation of capillary instabilities on a liquid jet. *J. Fluid Mech.* **168**, 479–500.
- LOSCERTALES, I. G., BARRERO, A., GUERRERO, I., CORTIJO, R., MARQUEZ, M. & GAÑÁN-CALVO, A. M. 2002 Micro/nano encapsulation via electrified coaxial liquid jets. *Science* **295**, 1695–1698.
- MONTANERO, J. M. & GAÑÁN-CALVO, A. M. 2008 Stability of coflowing capillary jets under nonaxisymmetric perturbations. *Phys. Rev. E* **77**, 046301.
- SANZ, A. & MASSEGUER, J. 1985 One-dimensional linear analysis of the compound jet. *J. Fluid Mech.* **159**, 55–68.
- SI, T., LI, F., YIN, X. & YIN, X. 2009 Modes in flow focusing and instability of coaxial liquid–gas jets. *J. Fluid Mech.* **629**, 1–23.
- STONE, H. A., STROOCK, A. D. & ADJARI, A. 2004 Engineering flows in small devices: microfluidics toward a lab-on-a-chip. *Annu. Rev. Fluid Mech.* **36**, 381–411.
- SURYO, R., DOSHI, P. & BASARAN, A. 2006 Nonlinear dynamics and breakup of compound jets. *Phys. Fluids* **18**, 082107.
- TOMOTIKA, S. 1935 On the instability of a cylindrical thread of a viscous liquid surrounded by another viscous liquid. *Proc. R. Soc. Lond. A* **150**, 322–337.
- UMBANHOWAR, P. B., PRASAD, V. & WEITZ, D. A. 2000 Monodisperse emulsion generation via drop break off in a coflowing stream. *Langmuir* **16**, 347–351.
- UTADA, A. S., FERNÁNDEZ-NIEVES, A., GORDILLO, J. M. & WEITZ, D. A. 2008 Absolute instability of a liquid jet in a coflowing stream. *Phys. Rev. Lett.* **100**, 014502 (1–4).
- UTADA, A. S., LORENCEAU, E., LINK, D. R., KAPLAN, P. D., STONE, H. A. & WEITZ, D. A. 2005 Monodisperse double emulsions generated from a microcapillary device. *Science* **308**, 537–541.